Journal of Hazardous Materials 511 (2026) 142260

Contents lists available at ScienceDirect

Journal of Hazardous Materials

journal homepage: www.elsevier.com/locate/jhazmat

Acetaminophen inhibits denitrification in *Paracoccus denitrificans*: Bioenergetic constraint and periplasmic electron transfer impairment

Zhi-Hui Dong [a], Yu Zhang [a,*], Jing Lu [a], Yi-Fan Zhu [a], Cheng-Jun Lu [a], Jian Yang [b], Zheng-Zhe Zhang [a], Ren-Cun Jin [a,*]

[a] *Zhejiang Provincial Key Laboratory of Wetland Intelligent Monitoring and Ecological Restoration, School of Engineering, Hangzhou Normal University, Hangzhou 310018, China*

[b] *Zhejiang Water Healer Technology Co., Ltd., Zhejiang, China*

HIGHLIGHTS

- APAP induces nitrite accumulation without serving as a C or N source.
- APAP inhibits denitrification by blocking ATPase proton translocation.
- *P. denitrificans* shifts metabolism to maintain ATPase efficiency.
- Cells prioritize PMF-driven iron uptake during energy limitation.

GRAPHICAL ABSTRACT

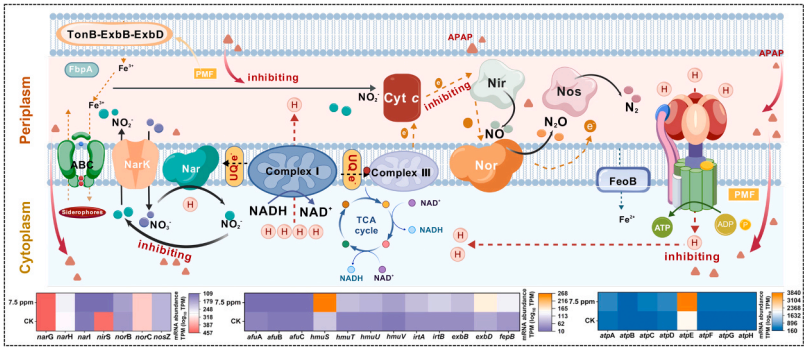

ARTICLE INFO

Keywords:
Acetaminophen
Bacterial denitrification
ATP synthesis
Electron Transport Chain
Municipal wastewater

ABSTRACT

Acetaminophen (APAP) is frequently detected in municipal wastewater, yet its effect on heterotrophic denitrification remains insufficiently resolved. Here, *Paracoccus denitrificans* was exposed to 0.5 and 7.5 ppm APAP, representing lower and higher wastewater-associated levels. Little change was observed at 0.5 ppm, whereas 7.5 ppm significantly depressed denitrification, with increased NO_2^- accumulation, higher N_2O emission, and slower bacterial growth. Intracellular ATP fell by 12.5%, and both $\Delta\Psi$ and ΔpH declined, indicating impairment of proton motive force homeostasis. The upstream membrane-associated electron transport system showed no significant change, but the periplasmic denitrification electron-transfer process was strongly inhibited. Docking analysis located APAP near the proton-channel region of ATPase, and the change in ATPase activity was consistent with impaired cellular energy conservation. These results indicate that APAP restricts heterotrophic denitrification mainly through bioenergetic constraint and impaired periplasmic electron transfer. The work provides a mechanistic basis for evaluating how pharmaceutical residues may weaken biological nitrogen removal in wastewater treatment systems.

* Corresponding authors.
E-mail addresses: yuzhang@hznu.edu.cn, yuzhang95@126.com (Y. Zhang), rcjin@hznu.edu.cn, jrczju@aliyun.com (R.-C. Jin).

https://doi.org/10.1016/j.jhazmat.2026.142260
Received 2 March 2026; Received in revised form 25 April 2026; Accepted 29 April 2026
Available online 30 April 2026

1. Introduction

Acetaminophen (APAP), also known as paracetamol or Tylenol, is one of the most widely used analgesics and antipyretics worldwide [1]. Its consumption increased markedly after the COVID-19 pandemic, and annual use has reached several thousand tons in some regions [1–3]. Meanwhile, APAP has been increasingly detected in municipal wastewater treatment systems [4], with reported concentrations ranging from below 0.1 ppb to more than 66.4 ppm [5,6]. Owing to its continuous input, high solubility, and biological toxicity [7,8], APAP has become a chemical pressure that deserves attention in municipal wastewater treatment systems.

Previous studies have mainly focused on the fate of APAP during nitrification. In biological nitrogen removal systems, APAP can be readily degraded under aerobic conditions. However, negative effects on sludge nitrification, especially nitrite oxidation, have also been reported [9–11]. APAP can be assimilated by heterotrophic microorganisms, and acetyl-CoA C-acetyltransferase and dihydrolipoyl dehydrogenase have been identified as key enzymes related to its biodegradation [12]. In addition to serving as a carbon source, APAP can also be oxidized to peroxynitrite by reactive nitrogen species (RNS) produced by nitrifying bacteria, such as •NO and free nitrous acid [13,14]. Even so, APAP removal is not always complete. Reported removal efficiencies range from 14.3% to 100% [5], suggesting that residual APAP is likely to enter downstream denitrification units [10,15–17].

Denitrification is another essential process in biological nitrogen removal from municipal wastewater. Once this process is incomplete, it inevitably leads to the accumulation of intermediates like NO_2^- and N_2O. N_2O is of particular concern because it is a potent greenhouse gas with a global warming potential 298 times that of CO_2 [18]. In comparison with nitrification, much less is known about the impact of APAP during denitrification. Available evidence remains limited and sometimes inconsistent. In a membrane reactor operated at a C/N ratio of 1.5, 0.5 ppm APAP had little effect on nitrate removal or nitrite accumulation in denitrifying sludge, and only a slight decrease was observed in the relative abundance of the dominant denitrifier, *Zoogloea* strain ZP7 [19]. In contrast, in a pure culture of *Zoogloea* strain ZP7, 0.25 ppm APAP was sufficient to suppress denitrification under low-carbon conditions (C/N = 2) by lowering membrane electron transport system activity, and cell growth was inhibited at the same time [20]. These observations suggest that the effect of APAP on denitrifying microorganisms may be masked in complex sludge systems. More importantly, it remains unclear how APAP interferes with denitrification-related electron transfer and why bacterial proliferation is inhibited simultaneously. A pure-culture system is therefore needed to obtain direct evidence for the way APAP disturbs the growth and metabolism of denitrifying bacteria.

Denitrification is fundamentally an anaerobic respiratory process driven by electron transport-coupled phosphorylation. On this basis, it was hypothesized that APAP-induced inhibition is associated with disruption of cellular bioenergetics. To test this hypothesis, mechanistic experiments were conducted using the model denitrifier *Paracoccus denitrificans* (ATCC 19367), which has been extensively studied and is commonly found in wastewater treatment plants [21–23]. Two treatment levels, 0.5 and 7.5 ppm, were selected to represent wastewater-associated exposure scenarios. Denitrification performance, intermediate accumulation, and bacterial proliferation were first evaluated. Cell membrane integrity, key denitrifying enzyme activities, cellular energy status, proton motive force, and electron-transfer characteristics were then examined. In addition, molecular docking was used to explore the potential inhibitory interaction between APAP and ATPase, and transcriptomic analysis was performed to identify transcriptional responses related to energy metabolism and denitrification. From a bioenergetic perspective, this study aims to clarify the basis of APAP-induced denitrification inhibition and the associated adaptive responses of denitrifying bacteria, and to provide further insight into the potential risk of pharmaceutical contamination to biological nitrogen removal processes.

2. Materials and methods

2.1. Chemicals and bacteria culture and batch experimental design

APAP ($C_8H_9NO_2$, CAS 103–90–2) was supplied by Sinopharm Chemical Reagent Co. Ltd. (China). A stock solution was prepared by dissolving 0.125 g APAP in 5 mL anhydrous ethanol. *P. denitrificans* (ATCC 19367) was acquired from the American Type Culture Collection. The strain was revived and grown to the logarithmic phase in the sterilized (121°C, 20 min) LB broth. Fresh cells were centrifuged (4°C, 6000 rpm, 5 min), washed 3 times by the sterilized phosphate-buffered saline (PBS, 12 mM, pH 7.4), and resuspended in PBS before batch tests.

Batch experiments were conducted in 100 mL glass flasks, each containing 50 mL sterilized denitrifying medium (pH 7.2) (See Supplementary Data, Text S1). To avoid amplifying the potential inhibitory effects of APAP due to nutrient limitation, the medium was supplied with sufficient sodium acetate as the initial carbon source (COD/NO_3^--N = 10) and supplemented with an appropriate amount of ammonium to support cell growth.

The APAP stock solution was added to achieve initial concentrations of 0.5 and 7.5 ppm in the denitrifying medium (See Supplementary Data, Text S2, Figure S1), representing lower and upper-end wastewater-associated exposure conditions within the reported concentration range of municipal WWTP influents [5]. After dilution, the corresponding final ethanol concentrations were approximately 0.02% (v/v) and 0.3% (v/v), respectively. To exclude potential confounding effects of the solvent, a separate ethanol vehicle-control group containing 0.3% (v/v) ethanol but without APAP addition was included. The vehicle-control data are provided in Supplementary Figure S2.

Prior to incubation, the initial cell optical density (A600) was adjusted to 0.06., the flasks were purged with N_2 (99.999%) for at least 3 min to remove dissolved oxygen, sealed with butyl stoppers, and incubated at 30°C with shaking at 150 rpm in the dark. Experiments were conducted in biological triplicate (n = 3).

2.2. Analytical methods

Samples were withdrawn every 2 h using a 2 mL sterile syringe, with 1.5 mL collected per sampling. Because the system was well-mixed, the extraction of small aliquots did not alter the concentrations or cell density of the remaining bulk liquid. Furthermore, all experimental groups (treatments and controls) were subjected to the identical sampling procedure; therefore, no mathematical volume correction was applied. Prior to measurement, liquid samples were passed through 0.45 μm membrane filters. The concentrations of NO_3^--N, NO_2^--N, and NH_4^+-N were determined using standard analytical procedures [24].

N_2O production was quantified by analyzing headspace gas samples using a gas chromatograph equipped with an electron capture detector (GC-ECD, Agilent 8860, USA) [25]. Calibration was performed using N_2O standard gas. Gas sampling was conducted at 2 h intervals. To ensure accurate quantification, the headspace pressure was equilibrated to atmospheric pressure prior to sampling. At each time point, 1 mL of headspace gas was manually withdrawn using a gas-tight syringe and immediately injected into the GC. The N_2O concentration was determined directly from the peak area based on the standard curve, with sampling-induced dilution accounted for.

RNS which primarily reflect NO and its related NO-derived species as mentioned previously, were quantified using the highly NO-specific fluorescent probe DAF-FM DA according to the standard fluorescence assay procedure (Beyotime, S0019). Because the formation of these reactive intermediate species is directly dependent on the presence of NO, the detected fluorescence signal serves as a reliable indicator to primarily represent intracellular NO levels. Harvested cells were washed

twice with 25 mM HEPES buffer (pH 7.5). The assay was performed in a 1 mL reaction system containing 100 μL of bacterial suspension (~10^7 cells) and DAF-FM DA at a working concentration of 5 μM. Incubation was carried out at 37°C for 20 min in the dark with intermittent vortexing every 5 min. A blank control without the probe was included to correct for background autofluorescence. Fluorescence intensity was recorded at excitation and emission wavelengths of 495 and 515 nm, respectively, and normalized to total protein concentration.

For the purpose of focusing on the evaluation of denitrification performance, total nitrogen (TN) was estimated by summing NO_3^--N, NO_2^--N, and N_2O-N. NO was not included in the TN calculation because it remained at extremely low levels without detectable accumulation during the denitrification process and was quantified using a fluorescence-based approach that is not directly comparable with mass-based measurements of NO_3^--N and NO_2^--N. Consequently, its contribution to TN was considered negligible [26].

2.3. APAP utilization analysis

Batch experiments were designed to examine the potential of APAP as a carbon and/or nitrogen source during denitrification. Carbon utilization was tested in acetate-free media, whereas APAP's role as a denitrification or assimilatory nitrogen source was evaluated in NO_3^-- or NH_4^+-free media, respectively (See Supplementary Data, Figure S3). Total organic carbon (TOC) and TN were determined using a total organic carbon analyzer (Analytik Jena, Germany). Acetate was quantified using a gas chromatography equipped with a flame ionization detector (GC-FID, Agilent 8860, USA) (See Supplementary Data, Text S3).

2.4. Cell viability and ATP content assay

The cell suspension (22 h) was washed twice with 12 mM PBS and resuspended. Cell viability was assessed using the Cell Counting Kit-8 (CCK-8, C0037, Beyotime, China). The cell suspension was incubated with the CCK-8 reagent (10:1, v/v) at 37°C for 30 min, and absorbance at 450 nm (A_{450}) was measured. To evaluate cell membrane integrity, lactate dehydrogenase (LDH) release was determined following previously reported methods [27,28].

Briefly, the cell suspension was centrifuged at 12000 rpm for 15 min at 4°C, and LDH activity in the supernatant was measured to assess the extent of membrane damage (See Supplementary Data, Text S4). ATP levels were determined using the BacTiter-Lumi ATP assay kit (C00658, Beyotime, China). The bacterial sample was mixed with the luminescence reagent (1:2, v/v) and incubated at 25°C for 10 min, and chemiluminescence intensity was recorded. The cell suspension was subsequently subjected to intermittent sonication (20 kHz, 5 min, 5 s intervals) in an ice-water bath using a cell disruptor. The lysate was centrifuged at 10000 rpm for 5 min at 4°C to remove debris, and the supernatant was collected for protein quantification by the Lowry method. All assays were performed in biological triplicate (n = 3).

2.5. Electron transport activities and denitrifying enzyme activities assay

To distinguish different levels of respiratory electron transfer during denitrification, electron transport system activity (ETSA) and periplasmic electron transport chain activity (PETCA) were measured separately in crude enzyme extracts. Cytochrome *c* (cyt *c*) content and ATPase activity were also determined (See Supplementary Data, Text S5). The crude enzyme extract was filtered through a 0.45 μm membrane before analysis.

PETCA was used as an operational measure of reduced cyt *c*-linked periplasmic denitrification process under the assay conditions. In the PETCA assay, reduced cyt *c* was supplied as the electron donor and NO_2^- as the electron acceptor. Because NO_2^- reduction in denitrification is followed by the formation and further reduction of downstream intermediates, including NO and N_2O, the decrease in reduced cyt *c* under the assay conditions was interpreted as reflecting the integrated periplasmic denitrification electron-transfer process initiated from NO_2^- reduction, rather than a single isolated reduction step.

The reaction mixture contained 12 mM PBS, 2 mM NO_2^-, 50 μM reduced cyt *c*, and crude enzyme extract. The reaction was carried out at 30°C, and the time-dependent changes of reduced cyt *c* and NO_2^- were monitored at 550 and 540 nm, respectively. The decrease in reduced cyt *c* was used as the primary readout of PETCA, while the decrease in NO_2^- was monitored to confirm that the reaction remained within the initial linear range (See Supplementary Data, Text S6). ETSA was determined separately as a membrane-associated electron transport parameter (See Supplementary Data, Text S7). All assays were performed in biological triplicate (n = 3).

Activities of nitrate reductase (NAR), nitrite reductase (NIR), nitric oxide reductase (NOR), and nitrous oxide reductase (NOS) were measured using crude enzyme extracts prepared from CK or APAP-exposed cells following established protocols [30], and APAP was not added to the reaction mixtures during the activity assays (See Supplementary Data, Text S8).

2.6. Molecular docking analysis

Molecular docking was simulated to investigate the interaction between APAP (PubChem CID 1983) and ATPase (PDB 5DN6). Protein preprocessing and docking simulations were carried out using PyMOL 2.4, AutoDock Tools 1.5.6, and AutoDock Vina 1.1.2 [29]. Putative binding poses between APAP and ATPase were prioritized based on binding energy and cluster frequency, and were used to suggest plausible contact regions. Docking visualizations were conducted using PyMOL 2.4 and PLIP (https://plip-tool.biotec.tu-dresden.de/plip-web/plip/index) [30].

2.7. RNA extraction, sequencing, and transcriptomic analysis

Cells were harvested after 22 h of cultivation and immediately flash-frozen in liquid nitrogen. Total RNA was isolated using the MiniBEST Universal RNA Extraction Kit (Takara, Japan). RNA concentration and purity were evaluated using a NanoDrop 2000 spectrophotometer (Thermo Scientific, USA), and RNA integrity was assessed using an Agilent 2100 Bioanalyzer (Agilent Technologies, USA). Only high-quality RNA samples were used for library construction. Sequencing libraries were generated and sequenced on the Illumina NovaSeq 6000 platform by Shanghai Majorbio Bio-pharm Technology Co., Ltd. (Shanghai, China). The raw transcriptomic sequence data generated in this study have been deposited in the NCBI BioProject database under accession number PRJNA1390485.

For bioinformatics analysis, raw data were quality-filtered using fastp (version 0.19.5) to remove adaptors and low-quality reads. Clean reads were mapped to the reference genome of *P. denitrificans* (NCBI Assembly ID: GCA_004063735.1) using Bowtie2 (version 2.3.5). Gene expression levels were quantified using RSEM (version 1.3.3) and normalized as transcripts per million (TPM). Transcriptomic comparison between treatments was conducted using the DEGseq package (version 1.38.0). Genes showing marked expression changes (adjusted $p < 0.05$ and $|\log_2 \text{fold change}| \geq 1$) were considered as significantly regulated. Functional annotation and enrichment analyses were performed based on the Gene Ontology (GO, Version 2022.0915) and Kyoto Encyclopedia of Genes and Genomes (KEGG, Version 2022.10) databases.

2.8. Other analytical methods

ΔpH and ΔΨ were determined using the pH-sensitive fluorescent probe BCECF-AM (Thermo Fisher, B1170, USA) and the membrane potential-sensitive probe JC-10 (Sigma-Aldrich, MAK160, USA), respectively (detailed in Supplementary Data, Text S9). All analyses

were conducted in triplicate, and the results are presented as means ± standard deviations. Statistical significance was evaluated using one-way analysis of variance (ANOVA) and *t*-tests by GraphPad Prism 9.5.0.

3. Results and discussion

3.1. Impact of APAP on denitrification performance

The effects of APAP on bacterial denitrification were assessed by monitoring TN removal efficiency (TNRE), NO_3^- and NO_2^- dynamics (expressed as normalized concentration ratios, C_t/C_0 and C_t/C_{0TN}, respectively), and N_2O emission. In the control check (CK) without APAP addition, *P. denitrificans* exhibited efficient denitrification, achieving a TNRE reaching 89.4% within 22 h (Fig. 1a), which is consistent with its well-documented high denitrification capacity under acetate-fed anoxic conditions.

Exposure to 0.5 ppm APAP did not significantly affect denitrification performance. In contrast, 7.5 ppm APAP markedly impaired denitrification. Specifically, TNRE dropped by 29.8%, and NO_3^- reduction was suppressed (Fig. 1b). Notably, NO_2^- reduction was the most sensitive to APAP stress. At 7.5 ppm APAP, the NO_2^- reduction rate decreased by 12.7%, resulting in pronounced NO_2^- accumulation (Fig. 1c). This inhibition coincided with a substantial increase in N_2O emission (Fig. 1d), consistent with previous studies [31], signaling a disruption in downstream denitrification processes. An ethanol vehicle-control experiment was further conducted to evaluate whether the solvent contributed to the observed inhibition. As shown in Supplementary Figure S1, the vehicle control showed no significant difference from CK in denitrification performance, indicating that the inhibitory effects observed in the 7.5 ppm APAP group were not attributable to the ethanol vehicle.

To evaluate whether reactive nitrogen species contributed to this inhibition, intracellular NO levels (a key component of RNS) were quantified using the NO-specific fluorescent probe DAF-FM DA. No significant changes in NO fluorescence were observed following exposure to 7.5 ppm APAP (Fig. 1e). At the peak of denitrification (18 h), the relative fluorescence intensity was 1.2 ± 0.1, statistically indistinguishable from the control ($p > 0.05$). This lack of variation indicates that NO-mediated toxicity or enzyme damage did not drive the accumulation of NO_2^- and N_2O. Alternative mechanisms, such as electron donor limitation, were also ruled out. Substrate utilization analysis revealed that APAP served neither as a carbon source nor as a nitrogen source for denitrification (See Supplementary Data, Figure S2).

In addition, the presence of APAP did not markedly affect the specific acetate consumption, which remained stable at approximately 2.9 mg COD/mg TN $_{re}$ (See Supplementary Data, Figure S2). These results confirm that neither toxic NO accumulation nor electron donor limitation caused the inhibition. Consequently, the deceleration in NO_2^- reduction likely stems from a direct disruption in the energy-generating machinery, specifically within the electron transport system or catalytic enzyme function.

3.2. Cell proliferation and viability

Membrane integrity and cell growth are generally considered indicators of the cellular energy state [32,33]. Accordingly, the LDH release and specific growth rate of *P. denitrificans* were analyzed. While exposure to 7.5 ppm APAP did not significantly alter the LDH release (Fig. 2a), underscoring that cell membrane integrity remained intact, it induced a distinct cytostatic effect (Fig. 2b). Specifically, the cell growth rate significantly reduced by 7.9% compared with CK (0.09/h), confirming a direct impediment to cell proliferation.

This suppressed biomass production was accompanied by preserved membrane integrity and reduced cell growth (Fig. 2a and b), suggesting that APAP did not primarily inhibit proliferation through membrane disruption. To further examine whether substrate assimilation was affected under this condition, the NH_4^+ uptake rate was quantified. Notably, the cellular NH_4^+ uptake rate remained stable at 0.06 mg N/(mg pro·h) under APAP treatment (Fig. 2c), indicating that ammonium

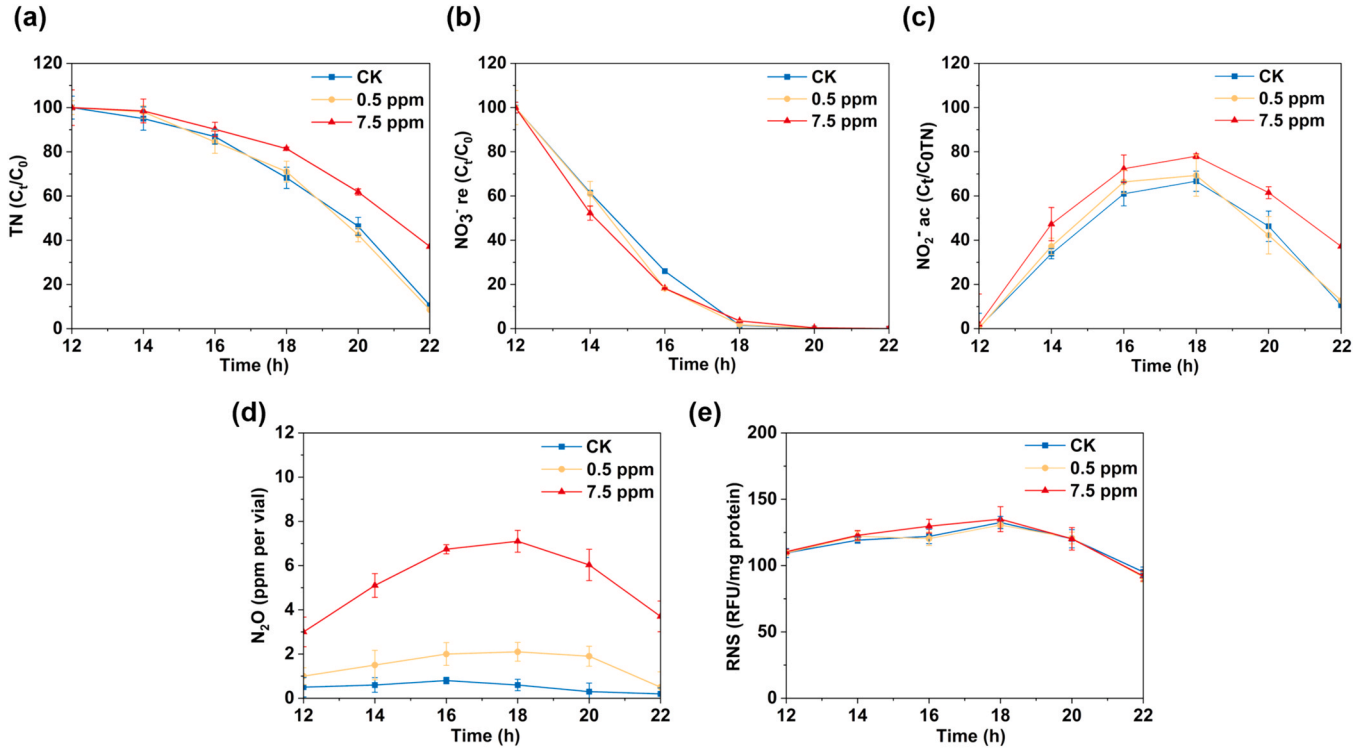

Fig. 1. Effects of APAP on TN removal (a), NO_3^- reduction (b), NO_2^- accumulation (c), emission profile of nitrous oxide (N_2O) (d), and intracellular RNS levels (e) during denitrification by *P. denitrificans*. Data are presented as mean ± SD (n = 3). NO_3^- reduction and NO_2^- accumulation are expressed as normalized concentration ratios (NO_3^- re (C_t/C_0), NO_2^- ac (C_t/C_{0TN})). Intracellular RNS levels are dominated by NO and expressed as relative fold change.

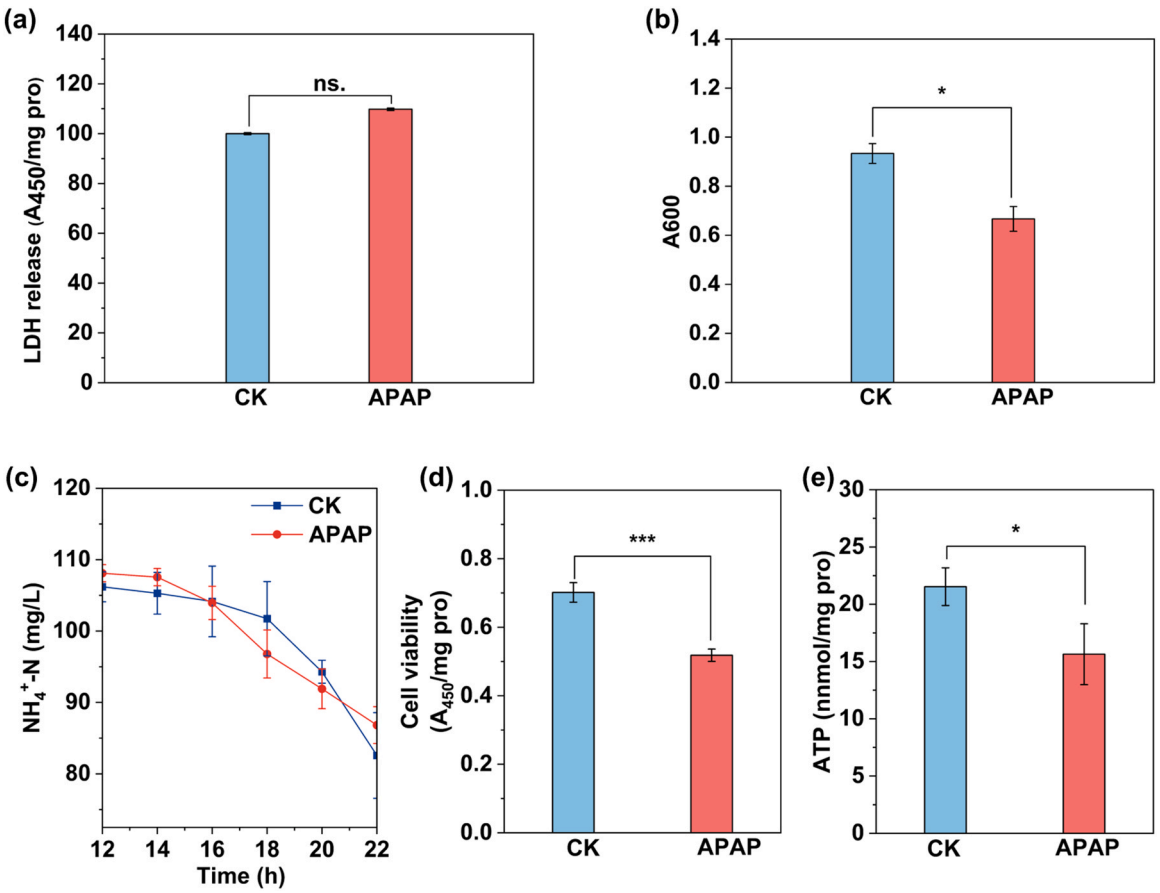

Fig. 2. Effects of APAP on LDH release (a), growth rate (b), the variation in NH_4^+-N concentration (c), cell viability (d), and ATP levels (e). The error bars represent the standard deviation. *, $p < 0.05$. ***, $p < 0.001$.

assimilation was not significantly impaired. Together with the marked decrease in intracellular ATP (Fig. 2e), these results suggest that APAP constrained cell proliferation primarily through impaired energy availability rather than through membrane disruption or insufficient ammonium assimilation.

As expected, APAP significantly reduced cell viability by 26.1% (Fig. 2d), suggesting that both substrate conversion efficiency and energy acquisition capacity were greatly impaired. ATP plays a critical role in biomass synthesis and maintaining cellular energy homeostasis [25, 34]. To determine whether APAP interfered with cellular energy metabolism, intracellular ATP levels were measured. The results revealed a significant 33.1% reduction in ATP content in the APAP-treated group (Fig. 2e), indicating that APAP severely impaired cellular energy production capacity.

Taken together, these results indicate that APAP suppresses bacterial proliferation not through membrane damage or substrate uptake inhibition, but primarily by constraining intracellular energy availability, thereby shifting cells toward an energetically conservative survival state.

3.3. Electron transfer disturbance and denitrifying enzyme activities

As illustrated in Fig. 3a, ETSA reflected the activity of the membrane-associated electron transport system, whereas PETCA represented the downstream periplasmic denitrification process. Exposure to 7.5 ppm APAP significantly inhibited PETCA by 59.2%, whereas ETSA did not show a significant change (Fig. 3b and S4). This contrast suggested that the detectable disturbance under APAP exposure was more evident in the periplasmic denitrification electron-transfer process than in the upstream membrane-associated electron transport system.

Similarly, the intrinsic NO_2^- reduction rate dropped by 57.1%. This enzymatic inhibition was notably more severe than the 12.7% decline in whole-cell NO_2^- removal. This discrepancy indicates that intact cells employ regulatory buffering mechanisms to maintain functional output despite impaired enzymatic capacity. Nevertheless, the impaired periplasmic electron-transfer process would still be expected to restrict the delivery of electrons to downstream nitrogen-oxide reduction steps, thereby contributing to the deterioration of denitrification performance and the accumulation of intermediates.

Consistent with impaired electron transport, the activities of key denitrifying enzymes were suppressed (Fig. 3b), and the magnitude of inhibition in crude extracts-measured with abundant artificial electron donors-suggests a compromised functional enzyme load rather than electron-supply limitation alone. The disparity between non-limiting electron availability and reduced extract activity indicates that the inhibition is rooted in the functional competency of the enzyme system rather than simple substrate accessibility. NAR activity decreased by 59.4% in crude extracts. Yet, this sharp *in vitro* decline contrasts with the relatively minor impact on *in vivo* NO_3^- removal, pointing to system-level buffering rather than a linear correlation between extract activity and whole-cell flux. In intact cells, NO_3^- reduction may not function as the rate-limiting step under the conditions examined. Thus, the pathway's intrinsic redundancy and metabolic plasticity can partially offset the observed reduction in NAR catalytic capacity.

Such buffering was much less evident during NO_2^- reduction, and NIR activity declined by 30.7%. Concurrently, transcriptomic analysis revealed significant downregulation of *nir*S, indicating that the NIR-catalyzed step was transcriptionally responsive to APAP exposure. Because NO_2^- reduction is both rate-limiting and highly dependent on electron supply, the system faces a dual constraint: reduced enzyme

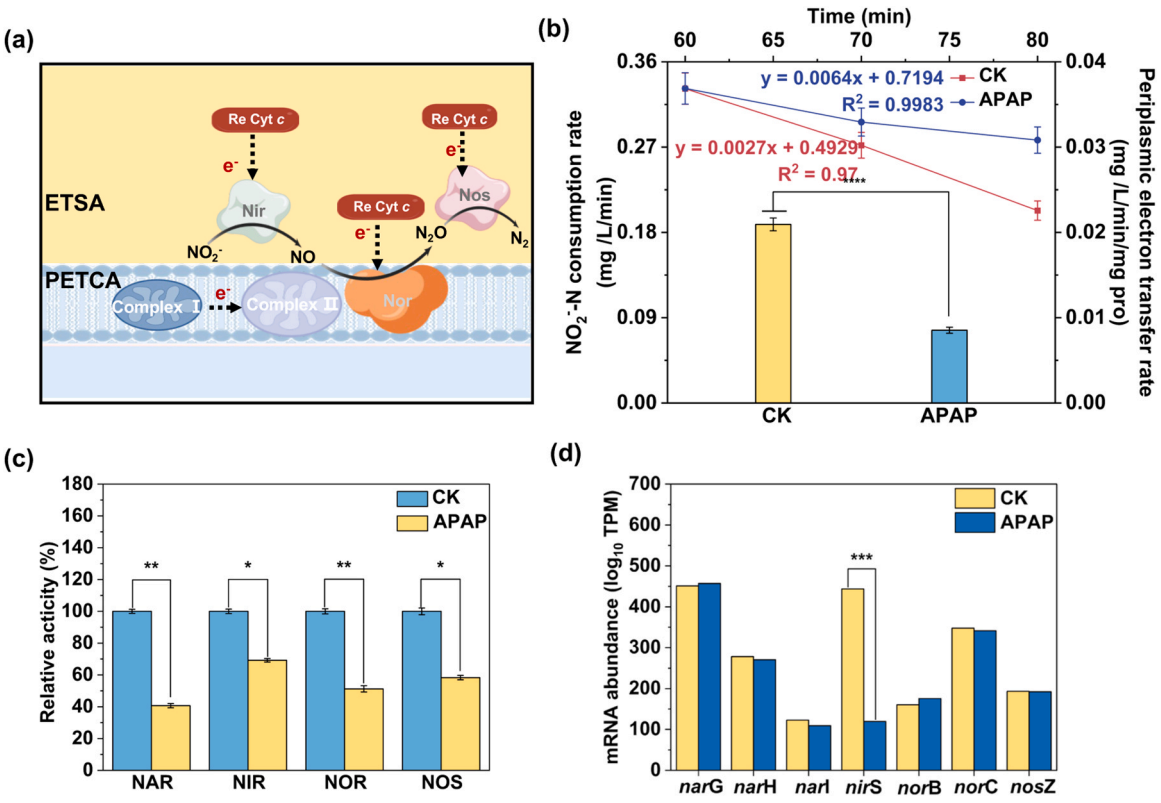

Fig. 3. Schematic illustration of the conceptual difference between electron transport system activity (ETSA) and periplasmic electron transport chain activity (PETCA) during denitrification (a), effects of APAP on PETCA (b), denitrifying enzyme activities (c), and nitrogen metabolism gene expression (d) in *P. denitrificans*. NAR, nitrate reductase; NIR, nitrite reductase; NOR, nitric oxide reductase; NOS, nitrous oxide reductase. *, $p < 0.05$; **, $p < 0.01$; ***, $p < 0.001$.

abundance and limited electron supply, its inhibition was likely intensified by the combined effects of reduced *nirS* transcription and

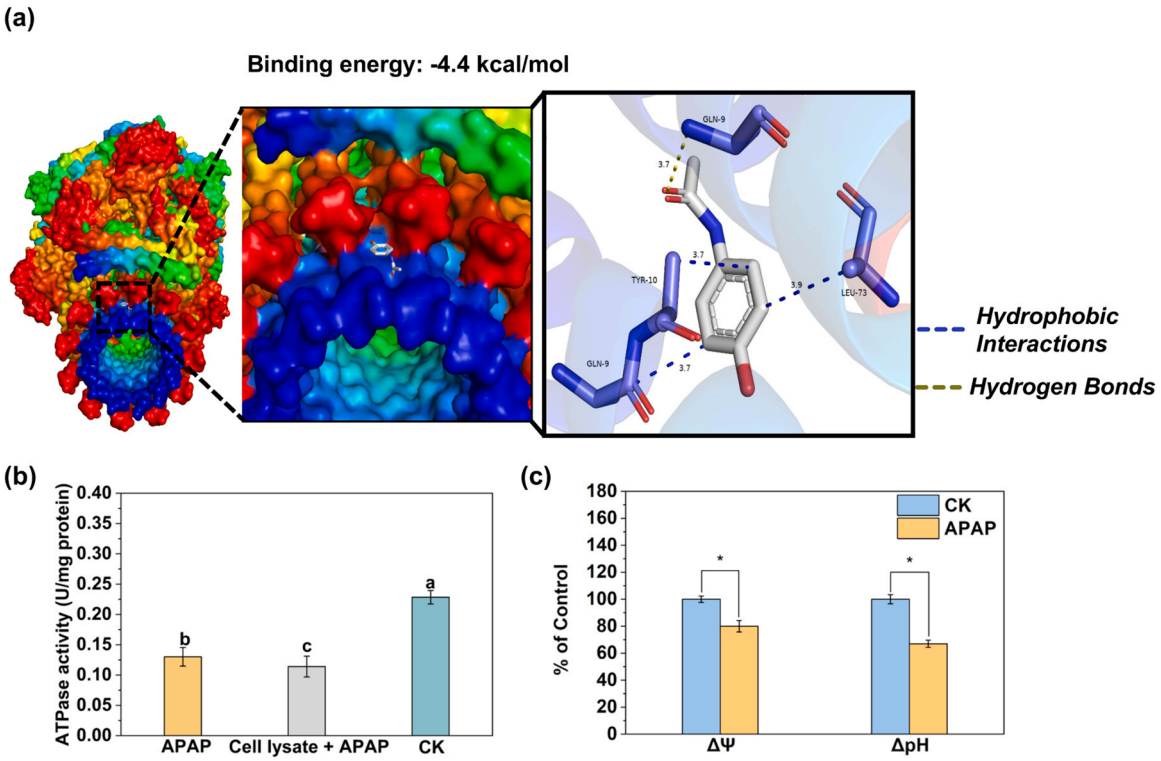

Fig. 4. Structural docking analysis illustrating the potential interaction between APAP and ATP synthase (a), ATPase activity under different treatments (b), and changes in membrane potential (ΔΨ) and transmembrane pH gradient (ΔpH) under APAP exposure (c). Data are presented as mean ± SD (n = 3).

restricted electron delivery. This greater vulnerability of the NO_2^- reduction step, relative to NO_3^- reduction, provides a direct explanation for the observed NO_2^- accumulation.

The activities of NOR and NOS were also significantly inhibited. In contrast to *nir*S, transcriptomic analysis showed no significant change in *nor*BC or *nos*Z expression, indicating that transcriptional regulation was less responsive at these downstream steps under APAP exposure. Meanwhile, periplasmic electron transport was strongly inhibited, which would be expected to restrict electron flow to both NOR and NOS in intact cells. Under this condition, the inhibition of NO and N_2O reduction can be reasonably interpreted as a downstream consequence of impaired periplasmic electron delivery.

However, no marked accumulation of cytotoxic NO was observed. This was likely because NO production was simultaneously constrained by the inhibition of the upstream NO_2^- reduction step, allowing the remaining NO reduction capacity to prevent toxic NO buildup under APAP stress. Collectively, these results indicate that APAP affected different denitrification steps through distinct regulatory responses, with NO_2^- reduction showing a clearer transcriptional response together with electron limitation, whereas the inhibition of downstream NO and N_2O reduction was more closely associated with impaired periplasmic electron transport under limited transcriptional response.

3.4. Function and expression of ATPase

To examine whether APAP could functionally interfere with ATP synthase-mediated proton translocation and thereby reduce ATP yield during denitrification, molecular docking analysis was employed to assess the structural plausibility of interactions between APAP and the ATPase complex. As shown in Fig. 4a, docking results indicate that APAP can adopt energetically favorable conformations within a pocket of the ATPase F_0 subunit located near the proton-channel region. The predicted lowest binding energy was −4.4 kcal/mol, indicating a low-affinity and transient interaction rather than a stable binding event. Notably, the top-ranked pose was positioned in close proximity to the narrow proton-conducting pathway [35], providing a reasonable structural context for potential functional interference. The interaction involved hydrogen bonding with Gln 9 J, as well as hydrophobic contacts with Gln 9 K, Tyr 10 K, and Leu 73 J.

Considering that molecular docking only provides structural plausibility, not direct functional evidence, ATPase activity was compared between intact cells exposed to APAP and cell lysates to which APAP was added after cell disruption. The results showed that ATPase activity measured in intact cells was significantly higher than that observed in APAP-treated cell lysates (Fig. 4b, $p < 0.05$). This finding indicates that disruption of cellular integrity exacerbates APAP-associated ATPase inhibition, This finding indicates that disruption of cellular integrity exacerbates APAP-associated ATPase inhibition, supporting the conclusion that APAP can directly impair ATP synthase function rather than acting solely through upstream metabolic or regulatory effects.

To directly evaluate whether APAP affected the proton motive force, both ΔΨ and ΔpH were measured under APAP exposure. As shown in Fig. 4c, exposure to 7.5 ppm APAP caused significant decreases in both ΔΨ and ΔpH, indicating that APAP disrupted the two major components of PMF. These data provide direct physiological evidence that APAP impaired PMF homeostasis, which is consistent with the observed decrease in intracellular ATP and supports the interpretation that APAP imposed a substantial bioenergetic constraint on denitrifying cells.

Taken together with the direct decreases in ΔΨ and ΔpH, these results indicate that APAP exposure was associated with substantial impairment of PMF and reduced ATP synthesis efficiency. Thus, the ATPase-related interference proposed here could be understood as a plausible upstream contributor to the observed bioenergetic disruption, rather than as an isolated interpretation based solely on docking. Because proton conduction within ATP synthase occurs through a spatially constrained pathway, even transient perturbations at this strategic location could elevate the energetic barrier for proton movement and thereby reduce the coupling efficiency between the proton motive force (PMF) and ATP synthesis, without requiring permanent or physical channel occlusion. Accordingly, these results suggest that APAP may weaken the efficiency with which ATP synthase converts the transmembrane electrochemical gradient into chemical energy, consistent with the observed decrease in intracellular ATP levels. Because APAP simultaneously suppresses respiratory electron transfer and associated proton pumping, the steady-state behavior of PMF cannot be inferred from ATP depletion and docking outcomes alone.

Notably, although ATP synthase-related genes (e.g., *atpF*), were transcriptionally upregulated under APAP exposure, no functional recovery of ATP synthase activity was observed. This discrepancy indicates that the increased gene expression likely reflects a stress-responsive adjustment rather than effective enzymatic compensation. Taken together with the docking-based structural indications of APAP occupancy in the proton-channel vicinity of the ATPase F_0 subunit, these findings support the hypothesis that APAP inhibits ATP synthase primarily by increasing the energetic barrier (or resistance) to proton translocation and lowering the coupling efficiency between PMF and ATP formation, rather than through a high-affinity allosteric inhibition mechanism.

3.5. Potential adaptive strategies

Under APAP-induced ATP depletion, cells experienced a severe energy shortage, where the limited ATP production could only sustain basic metabolic activities, failing to support cell proliferation. In response to this energy stress, *P. denitrificans* underwent significant metabolic reprogramming, adopting a resource reallocation strategy aimed at maximizing energy efficiency. This is most notably reflected in the restructuring of the energy-intensive iron transport system. Iron is not only a vital cofactor for key denitrification enzymes (NIR, NOR and NOS) [36] [37], but also plays a central role in establishing the transmembrane PMF [38–40], both of which are essential for maintaining basic electron flow.

Transcriptomic analysis revealed that the ATP-dependent iron transporter genes (*afu*ABC) were significantly down-regulated (Fig. 5a). In contrast, the PMF-dependent pathways were up-regulated, including the Ton-ExbBD complex (*fep*B) and heme-related iron transporters (*hmu*STUV, *irt*AB). By repressing energy-intensive ATP-dependent transporters and preferentially utilizing residual PMF for essential iron acquisition, cells could minimize direct ATP expenditure, thereby conserving energy for crucial survival functions. However, it should be noted that changes at the transcriptional level indicate a strategic metabolic adjustment rather than direct evidence of altered metabolic flux.

It should be noted that this transcriptional regulation reflects a relative shift in energy-coupling strategy under energy-limited conditions, rather than an enhancement or recovery of the transmembrane proton motive force itself. These changes suggested that *P. denitrificans* made a strategic metabolic adjustment by suppressing energy-intensive ATP-dependent iron transport systems while activating proton-motive-force-driven iron uptake pathways.

Importantly, the upregulation of PMF-dependent iron uptake pathways does not imply an enhancement or recovery of the proton motive force. Instead, under APAP-induced energy limitation, this shift reflects a relative, energy-sparing strategy in which cells preferentially reduce reliance on ATP-hydrolysis-driven transport and utilize residual PMF to sustain essential iron acquisition.

To validate whether the transcriptomic changes in iron acquisition were associated with physiological consequences, cyt *c* content was quantified as a representative iron-containing electron transfer protein. In a direct comparison between 2 APAP application modes, cyt *c* levels were significantly higher when APAP was applied to intact cells than when APAP was added after cell disruption ($p < 0.05$), indicating that

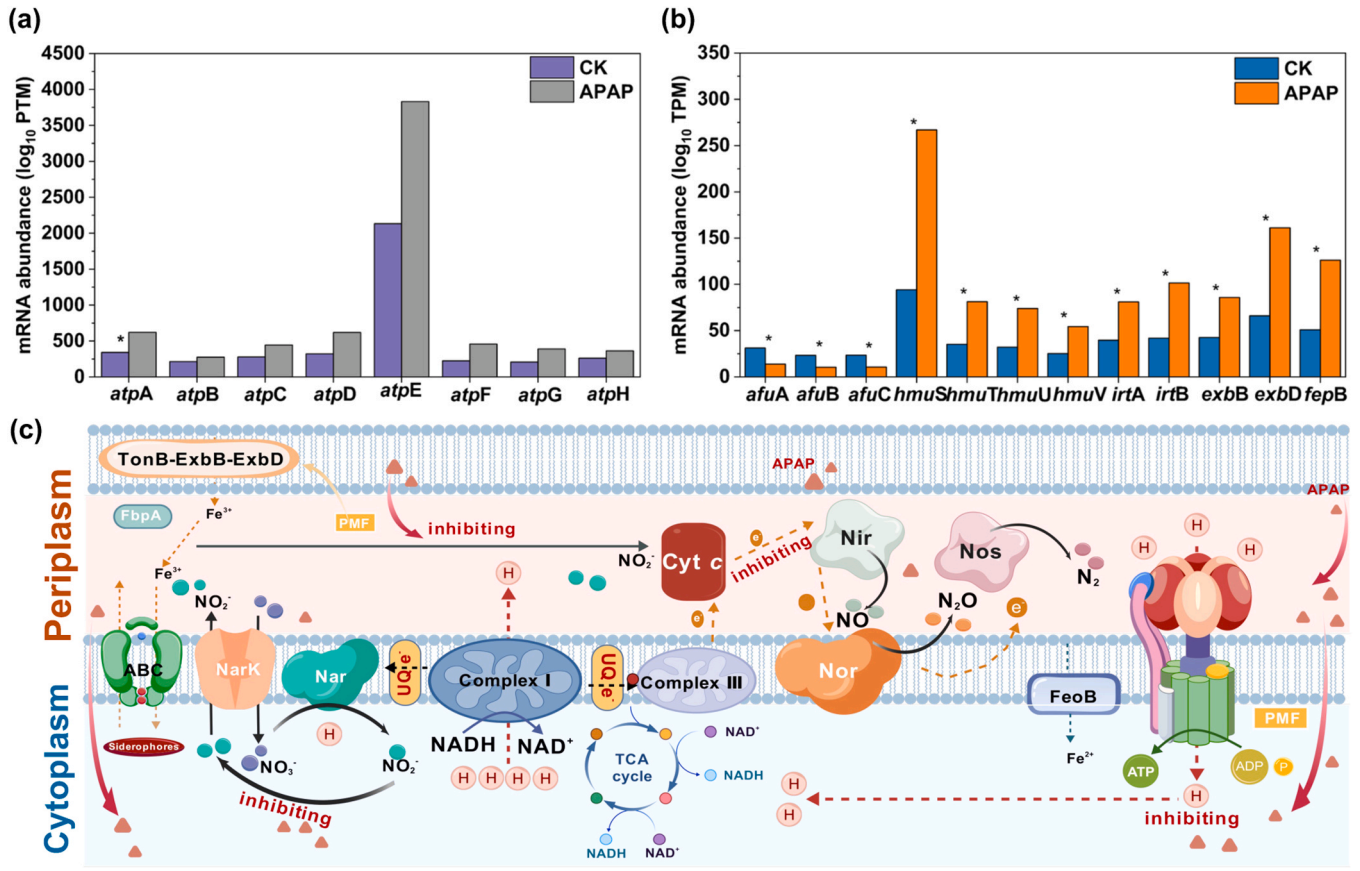

Fig. 5. Effects of APAP on the mRNA expression levels of functional genes in *P. denitrificans*, mRNA abundance (log_{10} TPM) of genes involved in iron transport (a) and F_1F_0-ATPase (*atp*A-H) (b). Metabolic inhibition and adaptive responses of denitrifying bacteria under APAP stress (c).

intact cellular organization partially buffers APAP-induced impairment of iron-dependent electron transport (See Supplementary Data, Figure S5). This observation is consistent with the down-regulation of ATP-dependent iron transporters (*afu*ABC) and the up-regulation of PMF-driven pathways, supporting an adaptive shift in iron acquisition under energy-limited conditions. By relying on proton gradients instead of ATP hydrolysis, these iron acquisition systems enabled efficient iron import with minimal energy expenditure, thereby conserving cellular ATP under energy-limited conditions.

Importantly, the upregulation of PMF-dependent transport pathways does not imply enhancement or recovery of PMF. On the contrary, direct measurements showed that both ΔΨ and ΔpH were significantly reduced under APAP exposure, demonstrating that PMF was substantially impaired. Under this ATP-limited and PMF-weakened condition, the upregulation of TonB-ExbBD is better interpreted as a relative energy-sparing adjustment, in which cells reduced reliance on ATP-hydrolysis-driven transport and preferentially utilized the residual proton motive force to sustain essential uptake processes. Together, these responses reflect the highly coordinated and dynamic adaptive capacity of *P. denitrificans* in reallocating critical resources to ensure survival under energy-limited conditions.

Given that microorganisms in natural and engineered systems are often exposed to suboptimal growth conditions and multiple co-occurring stresses, such energy-centered constraints may be further exacerbated in complex environments. Moreover, because ATP-dependent energy metabolism and adaptive resource reallocation are broadly conserved across microbial taxa, the energy-centric inhibitory mechanism identified here is likely not limited to *P. denitrificans*, but may also operate in diverse microbial communities, with potential implications for nitrogen removal and other energy-intensive biogeochemical processes.

4. Conclusion

APAP inhibited heterotrophic denitrification in *P. denitrificans* mainly through disturbance of cellular bioenergetics rather than through membrane damage or restricted substrate utilization. At 7.5 ppm, intracellular ATP, ΔΨ and ΔpH all declined, indicating impaired PMF homeostasis. The upstream membrane-associated ETSA changed little, whereas the *cyt* c-linked PETCA was clearly inhibited, accompanied by NO_2^- accumulation, increased N_2O emission, and reduced bacterial growth. Changes in ATPase activity, together with docking of APAP near the proton-channel region of ATPase, were consistent with impaired ATP synthesis as an upstream part of this response. Overall, the inhibition reflected a broader disturbance involving PMF impairment, restricted ATP generation, and inhibited periplasmic electron transfer, providing a mechanistic explanation for the susceptibility of biological nitrogen removal to pharmaceutical micropollutants.

Environmental Implication

As a frequently detected pharmaceutical in wastewater, acetaminophen may impair microbial nitrogen removal more than previously appreciated. In this study, acetaminophen disrupts denitrification by interfering with intracellular energy metabolism, which leads to nitrite accumulation and may increase the likelihood of nitrogen release from treated effluents. Such functional disruption can weaken wastewater treatment performance and potentially elevate eutrophication risk in receiving waters. The metabolic adaptations observed under chronic micropollutant exposure further suggest that microbial communities experience pronounced energetic constraints. Therefore, accounting for bioenergetic toxicity in environmental risk assessment frameworks is

necessary to better predict the ecological consequences of pharmaceutical contaminants originating from wastewater.

CRediT authorship contribution statement

Zheng-Zhe Zhang: Resources. **Jian Yang:** Formal analysis. **Cheng-Jun Lu:** Formal analysis. **Yi-Fan Zhu:** Formal analysis. **Yu Zhang:** Writing – review & editing, Supervision, Funding acquisition, Conceptualization. **Zhi-Hui Dong:** Writing – original draft. **Jin Rencun:** Writing – review & editing, Funding acquisition. **Jing Lu:** Formal analysis.

Declaration of Competing Interest

The authors declare that they have no known competing financial interests or personal relationships that could have appeared to influence the work reported in this paper.

Acknowledgments

This work was supported by the National Natural Science Foundation of China (No. 52500032) and the Zhejiang Provincial Natural Science Foundation of China (No. LQN26E080042 and LR20E080001).

Appendix A. Supporting information

Supplementary data associated with this article can be found in the online version at doi:10.1016/j.jhazmat.2026.142260.

Data Availability

Data will be made available on request.

References

[1] Yin, C.-F., Pan, P., Li, T., Song, X., Xu, Y., Zhou, N.-Y., 2025. The universal accumulation of p-aminophenol during the microbial degradation of analgesic and antipyretic acetaminophen in WWTPs: a novel metagenomic perspective. Microbiome 13 (1), 68. https://doi.org/10.1186/s40168-025-02065-2.

[2] Vieira, Y., Spode, J.E., Dotto, G.L., Georgin, J., Franco, D.S.P., dos Reis, G.S., et al., 2024. Paracetamol environmental remediation and ecotoxicology: a review. Environ Chem Lett 22 (5), 2343–2373. https://doi.org/10.1007/s10311-024-01751-1.

[3] Albarano, L., Maggio, C., Lofrano, G., Carotenuto, M., Guida, M., Vaiano, V., et al., 2025. Environmental risk assessment of paracetamol in aquatic ecosystems using species sensitivity distribution and global occurrence data. J Hazard Mater 499, 140107. https://doi.org/10.1016/j.jhazmat.2025.140107.

[4] Yu, C., Zhang, J., Fu, X., Zhou, B., Huang, J., Qin, J., et al., 2025. Wastewater-based monitoring of antipyretics use during COVID-19 outbreak in China and its associated ecological risks. Environ Res 267, 120680. https://doi.org/10.1016/j.envres.2024.120680.

[5] Wu, J.-l, Liu, Z.-h, Ma, Q.-g, Dai, L., Dang, Z., 2023. Occurrence, removal and risk evaluation of ibuprofen and acetaminophen in municipal wastewater treatment plants: a critical review. Sci Total Environ 891, 164600. https://doi.org/10.1016/j.scitotenv.2023.164600.

[6] Aydin, S., Aydin, M.E., Ulvi, A., 2019. Monitoring the release of anti-inflammatory and analgesic pharmaceuticals in the receiving environment. Environ Sci Pollut Res 26 (36), 36887–36902. https://doi.org/10.1007/s11356-019-06821-4.

[7] Zhao, Y., Yang, B., Liang, Z., Ji, H., Li, Z., 2026. New insights into the electron-transfer mechanism of Cr(VI) activation by carbon materials for simultaneously enhanced Cr(VI) detoxicate and acetaminophen oxidation: the role of defect structures. Water Res 292, 125301. https://doi.org/10.1016/j.watres.2025.125301.

[8] Tijani, J.O., Fatoba, O.O., Babajide, O.O., Petrik, L.F., 2016. Pharmaceuticals, endocrine disruptors, personal care products, nanomaterials and perfluorinated pollutants: a review. Environ Chem Lett 14 (1), 27–49. https://doi.org/10.1007/s10311-015-0537-z.

[9] Rios-Miguel, A.B., Smith, G.J., Cremers, G., van Alen, T., Jetten, M.S.M., Op den Camp, H.J.M., et al., 2022. Microbial paracetamol degradation involves a high diversity of novel amidase enzyme candidates. Water Res X 16, 100152. https://doi.org/10.1016/j.wroa.2022.100152.

[10] Dai, H., Gao, J., Shan, J., Lu, X., Li, D., Duan, W., et al., 2021. Pressure of high level acetaminophen on fixed biofilm and aerobic granule-based systems: insights on nitrification performances, microbial responses and acetaminophen's biodegradation pathways. Chem Eng J 426, 131907. https://doi.org/10.1016/j.cej.2021.131907.

[11] Xie, T., Gao, J., Zhang, Y., Guo, Y., Wang, H., Zhang, J., 2026. The merits of novel partial nitrification inhibitors: enhancing nitrogen removal performance while suppressing the spread of resistance genes in partial nitrification-anammox system. J Hazard Mater 508, 141939. https://doi.org/10.1016/j.jhazmat.2026.141939.

[12] Cui, Y., Gao, J., Gao, Y., Bao, F., Guo, Y., Zeng, L., et al., 2024. Identification of acetaminophen degrading microorganisms in mixed microbial communities using 13C-DNA stable isotope probing. Chem Eng J 487, 150656. https://doi.org/10.1016/j.cej.2024.150656.

[13] Chiron, S., Gomez, E., Fenet, H., 2009. Nitration processes of acetaminophen in nitrifying activated sludge. Environ Sci & Technol 44, 284–289. https://doi.org/10.1021/es902129c.

[14] Wang, N., Xu, Y., Peng, L., Liang, C., Song, S., Quintana, M., 2025. Biotic and abiotic removal of acetaminophen during sidestream partial nitritation processes: Underlying mechanisms and transformation pathways. Sci Total Environ 958, 177836. https://doi.org/10.1016/j.scitotenv.2024.177836.

[15] Phong Vo, H.N., Le, G.K., Hong Nguyen, T.M., Bui, X.-T., Nguyen, K.H., Rene, E.R., et al., 2019. Acetaminophen micropollutant: historical and current occurrences, toxicity, removal strategies and transformation pathways in different environments. Chemosphere 236, 124391. https://doi.org/10.1016/j.chemosphere.2019.124391.

[16] Shin, J., Lee, S., Lee, J., Son, H., Lee, Y., Mo Kim, Y., 2024. Impact of anaerobic zone on biodegradation of micropollutants: comparison of micropollutants' removal efficiencies in lab-scale anaerobic bioreactor and in full-scale anaerobic zone. Chem Eng J 481, 148356. https://doi.org/10.1016/j.cej.2023.148356.

[17] Saidulu, D., Bhatnagar, A., Gupta, A.K., 2025. Evaluating the role of different redox conditions on the removal of sulfamethoxazole, acetaminophen, and carbamazepine from wastewater: insights into biodegradation and sorption mechanisms. J Environ Chem Eng 13 (2), 116106. https://doi.org/10.1016/j.jece.2025.116106.

[18] Han, B., Yao, Y., Liu, B., Wang, Y., Su, X., Ma, L., et al., 2024. Relative importance between nitrification and denitrification to N2O from a global perspective. Glob Change Biol 30 (1), e17082. https://doi.org/10.1111/gcb.17082.

[19] Li, T., Li, X., Su, J., Liu, S., Bai, Y., Li, X., 2025. Development of a biofilm reactor using nano Fe3O4-modified biochar and red mud: Enhanced synergistic removal of nitrate, cadmium, and acetaminophen. Environ Res 287, 123142. https://doi.org/10.1016/j.envres.2025.123142.

[20] Li, T., Wang, Y., Qi, S., Su, J., Liu, S., Bai, Y., et al., 2025. Spent coffee grounds enhanced ferrous-driven microbial denitrification: synergistic removal mechanisms for nitrate and acetaminophen. J Environ Chem Eng 13 (6), 119701. https://doi.org/10.1016/j.jece.2025.119701.

[21] Peng, H., Zhang, Q., Su, Y., Wang, S., Chen, Y., 2025. Efficient denitrification and N2O mitigation in low-C/N wastewater treatment by promoting TCA cycle anaplerosis via glyoxylate shunt regulation. Nat Water 3, 992–1002.

[22] Wang, Y., Zhao, J., Bian, J., Li, R., Xu, S., Liu, R., et al., 2025. Hydrolytic dehalogenation of toxic haloacetic acids via carbon metabolism regulation during microbial denitrification. Environ Sci Technol 59 (22), 11121–11131. https://doi.org/10.1021/acs.est.5c04881.

[23] Leiviskä, T., Risteelä, S., 2022. Analysis of pharmaceuticals, hormones and bacterial communities in a municipal wastewater treatment plant – comparison of parallel full-scale membrane bioreactor and activated sludge systems. Environ Pollut 292, 118433. https://doi.org/10.1016/j.envpol.2021.118433.

[24] APHA, 2017. 2020 QUALITY ASSURANCE/QUALITY CONTROL. Standard Methods For the Examination of Water and Wastewater. American Public Health Association. https://doi.org/10.2105/SMWW.2882.015, 10.2105/SMWW.2882.015.

[25] Zhang, Y., Lu, J., Zhang, X.-Z., Zhang, Z.-Z., Jin, R.-C., 2025. PHA microplastic aging decreases N2O sink capacity: released γ-butyrolactone decouples denitrifying electron transfer and oxidative phosphorylation. Environ Sci Technol 59 (2), 1298–1307. https://doi.org/10.1021/acs.est.4c07717.

[26] Kellermann, R., Kumar, S., Gates, A.J., Bakken, L., Spiro, S., Bergaust, L., 2025. The flavohemoglobin hmp and nitric oxide reductase restrict initial nir expression in the bet-hedging denitrifier paracoccus denitrificans by curtailing hypoxic NO signalling. Environ Microbiol 27 (3), e70079. https://doi.org/10.1111/1462-2920.70079.

[27] Wan, R., Chen, Y., Zheng, X., Su, Y., Li, M., 2016. Effect of CO2 on microbial denitrification via inhibiting electron transport and consumption. Environ Sci Technol 50 (18), 9915–9922. https://doi.org/10.1021/acs.est.5b05850.

[28] Zhang, L., Narita, Y., Gao, L., Ali, M., Oshiki, M., Ishii, S., et al., 2017. Microbial competition among anammox bacteria in nitrite-limited bioreactors. Water Res 125, 249–258. https://doi.org/10.1016/j.watres.2017.08.052.

[29] Trott, O., Olson, A.J., 2010. AutoDock Vina: improving the speed and accuracy of docking with a new scoring function, efficient optimization, and multithreading. J Comput Chem 31 (2), 455–461. https://doi.org/10.1002/jcc.21334.

[30] Adasme, M.F., Linnemann, K.L., Bolz, S.N., Kaiser, F., Salentin, S., Haupt, V.J., et al., 2021. PLIP 2021: expanding the scope of the protein-ligand interaction profiler to DNA and RNA. Nucleic Acids Res 49 (W1), W530–W534. https://doi.org/10.1093/nar/gkab294.

[31] Bruman, S.M., Zubareva, V.M., Shugaeva, T.E., Lapashina, A.S., Feniouk, B.A., 2025. Activation of bacterial F-ATPase by LDAO: deciphering the molecular mechanism. Biochemistry 90 (3), 374–388. https://doi.org/10.1134/S0006297924602600.

[32] Shi, H.-T., Zeng, Q.-Y., Feng, X.-C., Xiao, Z.-J., Jiang, C.-Y., Wang, W.-Q., et al., 2024. How denitrifiers defense ciprofloxacin: insights from intracellular and

extracellular stress response. Water Res 259, 121851. https://doi.org/10.1016/j.watres.2024.121851.
[33] Wan, R., Wang, L., Chen, Y., Zheng, X., Chew, J., Huang, H., 2019. Tetrabromobisphenol A (TBBPA) inhibits denitrification via regulating carbon metabolism to decrease electron donation and bacterial population. Water Res 162, 190–199. https://doi.org/10.1016/j.watres.2019.06.046.
[34] Shi, H.-T., Feng, X.-C., Xiao, Z.-J., Wang, W.-Q., Wang, Y.-M., Zhang, X., et al., 2022. Analysis of the β-cyclodextrin enhancing bio-denitrification from the perspective of substrate metabolism, electron transfer, and iron acquisition. Chem Eng J 446, 137358. https://doi.org/10.1016/j.cej.2022.137358.
[35] Sielaff, H., Duncan, T.M., Börsch, M., 2018. The regulatory subunit ε in Escherichia coli FOF1-ATP synthase. Biochim Et Biophys Acta (BBA) - Bioenerg 1859 (9), 775–788. https://doi.org/10.1016/j.bbabio.2018.06.013.
[36] Olaya-Abril, A., Hidalgo-Carrillo, J., Luque-Almagro, V.M., Fuentes-Almagro, C., Urbano, F.J., Moreno-Vivián, C., et al., 2018. Exploring the denitrification proteome of paracoccus denitrificans PD1222. Front Microbiol 9, 2018. https://doi.org/10.3389/fmicb.2018.01137.
[37] Glass, J.B., Elbon, C.E., Williams, L.D., 2023. Something old, something new, something borrowed, something blue: the anaerobic microbial ancestry of aerobic respiration. Trends Microbiol 31 (2), 135–141. https://doi.org/10.1016/j.tim.2022.08.006.
[38] Koebke, K.J., Pinter, T.B.J., Pitts, W.C., Pecoraro, V.L., 2022. Catalysis and electron transfer in De Novo designed metalloproteins. Chem Rev 122 (14), 12046–12109. https://doi.org/10.1021/acs.chemrev.1c01025.
[39] Peng, Y., He, S., Wu, F., 2021. Biochemical processes mediated by iron-based materials in water treatement: enhancing nitrogen and phosphorus removal in low C/N ratio wastewater. Sci Total Environ 775, 145137. https://doi.org/10.1016/j.scitotenv.2021.145137.
[40] Seyoum, Y., Baye, K., Humblot, C., 2021. Iron homeostasis in host and gut bacteria – a complex interrelationship. Gut Microbes 13 (1), 1874855. https://doi.org/10.1080/19490976.2021.1874855.